Spin Transfer Torque in Graphene-based Domain Walls

Z. Rashidian[*1], Kh. Jahanbani[2]
1. Department of Physics, Lorestan University, Khoramabad 68151-44316, Iran
2. Department of Materials Science and Engineering, School of Engineering, Meybod University, Yazd, 89616-99557, Iran

E-mail: rashidian.z@lu.ac.ir

Abstract
Scattering matrix formalism is employed to calculate the spin transfer torque in a graphene-based domain wall (DW) in the ballistic regime. We have suggested a new method for manipulating the direction of domain wall motion by both the length of the DW and magnetic barrier that is the ratio of induced exchange field to Fermi energy. It has also shown that spin current density gives us more insight into the transmission of spin-polarized electrons.

Keywords: machine, machine, machine, machine, machine, machine, machine

1. Introduction

In the burgeoning and progressive field of spintronics1, 2 magnetic materials have drawn much attention in light of having intriguing physics, non-volatile nature, and enormous applications in modern technology3.
Graphene4, 5, 6 the newly two-dimensional allotrope of carbon atoms with rich potential such as weak spin-orbit coupling, rather long spin-flip length at room temperature7, spin-polarized current lifetimes and Klein tunneling8 is a good candidate for magnetic materials in particular in the field of spintronics.
However neutral graphene is not magnetic originally, but it has the potential to be ferromagnetic. Ferromagnetism in graphene is induced intrinsically9 as well as extrinsically by means of various applied stimuli such as proximity effects by magnetic gates10 and spin injection in graphene7. Recently, spin-transfer torque (STT) in a graphene system with the presence of spin-orbit coupling (SOC) has been theoretically studied11.
Information is written by switching magnetic textures such as magnetization of the conventional magnetic memory devices to the desired configuration with nonlocal magnetic fields. With the development of information technology, for the miniaturization of magnetic read heads and random access memory (RAM) elements and more importantly, having high capacity of magnetic devices, higher and cumbersome magnetic fields is required.
In pursuit of a new mechanism for circumventing this problem without referring to magnetic fields, spin transfer torque is realized as a novel magnetization switching mechanism. Recently, the intriguing possibility of manipulating high-density nonvolatile magnetic device elements without applying high magnetic fields12 has been reported that leads to magnetic switching with currents. Spin transfer torque (STT) that arises due to non-conservation of spin angular momentum of spin-polarized electrons while crossing the ferromagnetic region, was first pointed out by Berger13 in the case of DW and Slonczewski14.
From many magnetic patterns, DW is considered as a structure with high potential for technological applications. It has been suggested that devices based on DWs could be applied for information carriers in memory and logic devices15,16 (each wall represents a single bit). DW racetrack memory proposed by Parkin is one possibility.
for high density storage17,18 it has also theoretically19 and experimentally20,21 verified that Spin transfer torque could cause DW motion and moreover it is presently employed as a means of control of the DW motion in device applications for non-volatile memory22.
Calculating the spin transport torque on the DW system (GaMnAs)23 and the current-induced DW's motion of a DW24, 25 has been reported. Recently, a great deal of attention on spin transfer torque in graphene systems has been made27, 28.
It is the purpose of the present paper to explore the spin transfer torque on the graphene based DW, analytically. Actually, we will find a way to manipulate the DW motion with the direction of STT with factors such as the exchange field and the length of the DW. In the case of graphene systems with the presence of anomalous Klein tunneling phenomena that changes the conductance in the graphene-based DW significantly, we are stimulated to explore also the influences of this phenomena on the spin transfer torque.
Since having high domain wall velocity29 associated with low critical current density is the aim of the theoretical research, we suggest graphene as a potential material

system for applying as a racer due to the feasibility of manipulating its magnetization and then having less spin current density for switching or reversal state of the moment.

2. Model

We begin with a structure consisting of an all graphene ferromagnetic - domain wall - ferromagnetic (FM-DW-FM) junction as shown schematically in Fig. 1. The system consists of a left ($x < 0$) and right ($x > L$) semi-infinite FM leads separated by a π DW. We can think of ferromagnetic regions, whose magnetizations are oppositely aligned, as two reservoirs of spin-polarized electrons.

Here we consider a Bloch type domain wall i.e., the exchange field rotates linearly in the $x - z$ plane, with an angle θ w.r.t the z -axis as: $h(x) = h\ cos\,\theta\,(x)\hat{e}_z + h\ sin\,\theta\,(x)\hat{e}_x$, while the graphene sheet is deposited in the $x - y$ plane. Here $\theta(x) = \pi x/L$ in DW and $\theta = 0$ ($\theta = \pi$) in the left (right) leads.

Our description of the system relies on the low energy Dirac-like Hamiltonian that is subjected to an exchange field $\boldsymbol{h}(x)$ in a free electron stoner model. This Hamiltonian in the presence of gauge potentials can be written as a Kronecker product between the 2×2 pauli matrices in different space as follows:

$H = v_F\,\pi.\tau \otimes \sigma^0 - \tau^0 \otimes \sigma.h(x)$
$-E_F\tau^0 \otimes \sigma^0$ (1)

Where v_F is the Fermi velocity, E_F is the Fermi energy and σ^0 and τ^α ($\alpha = 0, x, y, z$) are four components of the Pauli matrices acting on real spin and pseudospin degrees of freedom, respectively. Canonical momentum in the 4×4 space reads:

$\pi_i = p_i\tau^0 \otimes \sigma^0 + A_i^\alpha\ \tau^0 \otimes \sigma^\alpha$ (2)

Here a sum over repeated index α is implies, $i = x, y, z$ are spatial components and A_i^α is a component of the vector ($\alpha = 0$) and $SU(2)$ gauge ($\alpha \neq 0$) potentials31. The charge ($\alpha = 0$) and spin ($\alpha = x, y, z$) current densities could be defned through the derivative of the Hamiltonian (1) with respect to the gauge potentials:

$J_i^\alpha = \frac{\delta\langle H\rangle}{\delta A_i^\alpha} = v_F\Psi^\dagger(\tau^0 \otimes \sigma^\alpha)(\tau^i \otimes \sigma^0)\Psi.$ (3)

Similarly, we can defne the charge and spin densities as

$S^\alpha\ \Psi^\dagger\tau^0 \otimes \sigma^\alpha\Psi.$ (4)

In Eqs. (3) and (4), $\Psi^\dagger = (\psi^*_{A,\uparrow}, \psi^*_{B,\uparrow}, \psi^*_{A,\downarrow}, \psi^*_{B,\downarrow})$ is the four-component eigenvector. Note that $S^0 = \Psi^\dagger\tau^0 \otimes \sigma^0\Psi = \Psi^\dagger\Psi$ is the particle density n. Since in our FDW-F structure the only relevant spatial component is the x-direction, for simplicity we defne

$Q^\alpha = J_x^\alpha = v_F\Psi^\dagger(\tau^x \otimes \sigma^\alpha)\Psi.$ (5)

for the x-component of the current. The spin current density is tensor ,i.e., has a flow direction and a polarization, we suppress the index of x-direction in the real space and just write its direction in spin space hereafter.

A spin up incoming plane wave having unit incident particle flux (in the upper band) reads:

$$\Psi_{in} = \frac{1}{\sqrt{cos\ (\alpha^\uparrow)}}\begin{pmatrix} e^{-i\alpha^\uparrow/2} \\ e^{i\alpha^\uparrow/2} \\ 0 \\ 0 \end{pmatrix} e^{ik^\uparrow x}$$

Reflected and transmitted components of the wavefunction also read

$$\Psi_r = \frac{r^{\uparrow\uparrow}e^{-ik^\uparrow x}}{\sqrt{\cos(\alpha^\uparrow)}}\begin{pmatrix} e^{\frac{i\alpha^\uparrow}{2}} \\ -e^{-\frac{i\alpha^\uparrow}{2}} \\ 0 \\ 0 \end{pmatrix} + \frac{r^{\downarrow\uparrow}e^{-ik^\downarrow x}}{\sqrt{cos\ (\alpha^\uparrow)}}\begin{pmatrix} 0 \\ 0 \\ e^{i\alpha^\downarrow/2} \\ -e^{-i\alpha^\downarrow/2} \end{pmatrix} \quad (7)$$

$$\Psi_t = \frac{r^{\uparrow\uparrow}e^{-ik^\downarrow(x-L)}}{\sqrt{\cos(\alpha^\downarrow)}}\begin{pmatrix} e^{-\frac{i\alpha^\downarrow}{2}} \\ e^{\frac{i\alpha^\downarrow}{2}} \\ 0 \\ 0 \end{pmatrix} + \frac{r^{\downarrow\uparrow}e^{-ik^\uparrow(x-L)}}{\sqrt{cos\ (\alpha^\uparrow)}}\begin{pmatrix} 0 \\ 0 \\ e^{-i\alpha^\uparrow/2} \\ e^{i\alpha^\uparrow/2} \end{pmatrix} \quad (8)$$

Here $t^{\downarrow\uparrow}$ ($r^{\downarrow\uparrow}$) are the transmission (reflection) probability from up to down spin(spin flip from its original orientation)and $t^{\uparrow\uparrow}$ ($r^{\uparrow\uparrow}$) are those of without spin flip, respectively. Where we have defned the wave vectors in the leads:

$k^\uparrow L = k_F L\left(\Xi + 1 + \frac{h}{E_F}\right)cos(\alpha^\uparrow),$

$k^\downarrow L = k_F L\left(\Xi + 1 - \frac{h}{E_F}\right)\ cos(\alpha^\downarrow)$

And we have. $\Xi = \varepsilon/E_F$. Here ε is the quasiparticle energy measured from the Fermi energy that we have taken zero. $\alpha^\uparrow(\alpha^\downarrow)$ is the incidence angle for up (down)-spin electrons with respect to the x-axis.

Wavefunctions in the DW region is obtained with transforming spinors to a rotating frame30 for changing the quantization axis. $R(\theta)$ is a spin-rotation operator, given by

$$R(\theta) = \tau^0 \otimes e^{-\frac{i\sigma_y\theta}{2}} = \tau^0 \otimes \begin{pmatrix} cos\frac{\theta}{2} & -sin\frac{\theta}{2} \\ sin\frac{\theta}{2} & cos\frac{\theta}{2} \end{pmatrix}$$

The wavefunction in the DW region ($0 \leq x \leq L$) is too cumbersome to be mentioned here. After writing the similar expressions for incoming down-spin electrons, the total transmission and reflection probabilities are determined from imposing the continuity conditions at the interfaces ($x = 0$ and $x = L$):

$\Psi_{Left}\ (x = 0) = \Psi_{DW}(x = 0),$
$\Psi_{Right}(x = L) = \Psi_{DW}\ (x = L)$

We study spin transfer torque that is a vector in spin space with considering the net changes in the spin current transmitted with reflected and incident20, 23, 24, 27.The spin transfer torque exerted on the magnetization in the DW region is obtained with net spin flux from the DW as:

$N_x = Q_{in}.\hat{X} - (Qt.\hat{X} + Q_R.(-\hat{X}))$

Spin current density for reflected spin-polarized electrons reads:

$$Q_R = (\tau_s^i)_R = 2\frac{1}{2}\Sigma_s\int_0^{\pi/2}\psi_R^\dagger\tau_x \otimes \sigma^i\psi_R d_{\alpha^s}$$

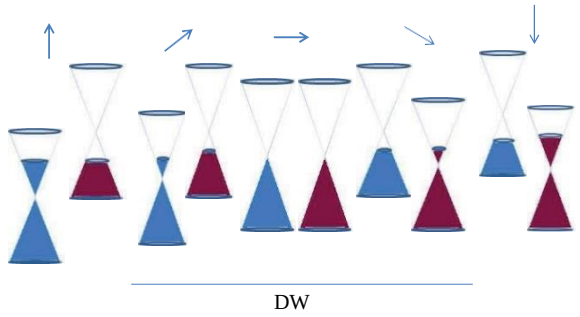

FIG. 1: Color online: Schematic structure of the spin-up and spin-down subbands and direction of the exchange felds (in the $x-z$ plane)

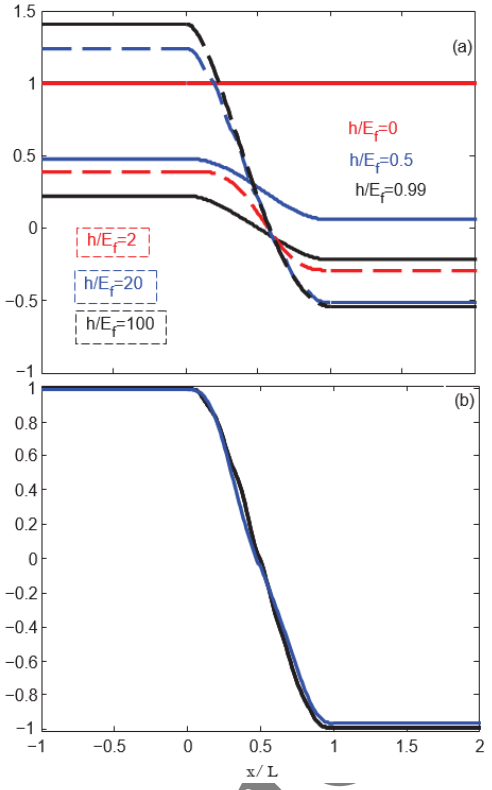

FIG.2: Color online: Spin current density of spin polarized carriers in the z direction ves location of the DW region normalized to the length of the DW region. $k_F L = 1$ and $k_F L = 10$ for panel (a) and (b).

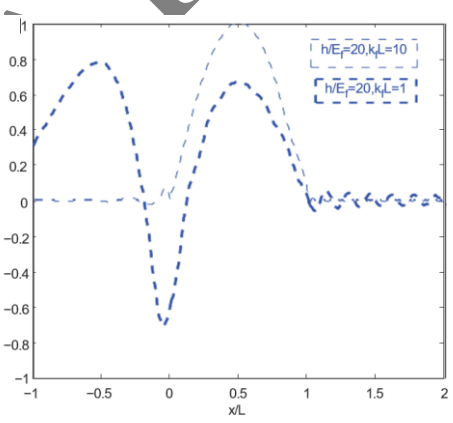

FIG.3: Color online: Spin current density of spin polarized carriers in the $x-$ direction versus location of the DW region normalized to the length of the DW region.

Summation on s is over up and down spin incoming electrons. We have similar expressions for the spin current density of the incident and transmitted electrons.
The obtained spin torque is a variable of the magnetic barrier (ratio of exchange field to Fermi energy) and the length of the DW region. The current direction is along the x-axis, then there are just three components of the spin transfer torque tensor as follows:

$$N_{xx} = \frac{-2\cos\left(\frac{\alpha^{\uparrow}+\alpha^{\downarrow}}{2}\right)}{\sqrt{\cos\alpha^{\uparrow}\cos\alpha^{\downarrow}}}\left[\left(r^{\uparrow\uparrow}r^{\downarrow\uparrow\dagger}+r^{\uparrow\uparrow\dagger}r^{\downarrow\uparrow}\right)+ t^{\uparrow\uparrow}t^{\downarrow\uparrow\dagger}e^{iL(k^{\downarrow}-k^{\uparrow})}+t^{\uparrow\uparrow\dagger}t^{\downarrow\uparrow}e^{-iL(k^{\downarrow}-k^{\uparrow})}\right] \quad (11)$$

$$N_{yx} = \frac{-2i\cos\left(\frac{\alpha^{\uparrow}+\alpha^{\downarrow}}{2}\right)}{\sqrt{\cos\alpha^{\uparrow}\cos\alpha^{\downarrow}}}\left[\left(-r^{\uparrow\uparrow}r^{\downarrow\uparrow\dagger}+r^{\uparrow\uparrow\dagger}r^{\downarrow\uparrow}\right)+ t^{\uparrow\uparrow}t^{\downarrow\uparrow\dagger}e^{iL(k^{\downarrow}-k^{\uparrow})}-t^{\uparrow\uparrow\dagger}t^{\downarrow\uparrow}e^{-iL(k^{\downarrow}-k^{\uparrow})}\right] \quad (12)$$

$$N_{zx} = 2\left[1-r^{\uparrow\uparrow}r^{\uparrow\uparrow\dagger}-t^{\uparrow\uparrow}t^{\uparrow\uparrow\dagger}+t^{\downarrow\uparrow}t^{\downarrow\uparrow\dagger}+r^{\downarrow\uparrow}r^{\downarrow\uparrow\dagger}\right] \quad (13)$$

3. Conclusion

In conclusion, we have evaluated the spin current density (SCD) and spin-transfer torque within a scattering approach using Landauer Buttiker formula for all graphene FM-DW-FM structure.
We have plotted the z-component of spin space of (spatially dependent) SCD induced by the spin-polarized electrons versus its location in the $x-$ direction in real space. The results show the behavior of SCD for carriers crossing the DW region in the direction of its flow ($x-$ axis). The minus sign for x-axis indicates the incoming region and from $x = 0$ to $\frac{x}{L} = 1$ is related to the DW region and after it shows the transmitted region.
As follows from Fig. 2(a) and Fig. 3 for $k_F L = 1$ a bit rotation of spin in the plane of $x - z$ is seen, i.e., the spin could not have the opportunity to follow the exchange field adiabatically in the DW region, while according to Fig. 2(b) that pertains to the high value of $k_F L = 10$ for every nonvanishing value of magnetic barrier, perfect rotation of spin occurs, as expected. In this case, as one infers from Figs. 3 and 2 for instance in the middle region of DW, the direction of spin polarization of the current coincides itself with the exchange field, i.e., the $x-$ component of traversing spin lies on the $x-$ axis without having $z-$ component in spin space. Strictly speaking, spin current density give more insight into the transport of spin-polarized electrons.
In general, the electric current moving through the DW region manifests its effects as both the adiabatic torque32 exert on the wall in the direction of x, $(\vec{v}_s.\nabla)\vec{h}(r)$ as shown in Fig. 4 as well as non-adiabatic torque33 $\beta\vec{h}(r)\times(\vec{v}_s.\nabla)\vec{h}(r)$ in the direction of y as represented in Fig. 5, where v_s is proportional to the current density and the conduction electron spin polarization. The mentioned torques also called the in-plane and out of plane (plane of rotating magnetization) torque, respectively. Both of theses effects have crucial role in the domain wall motion but in different ways. According to Ref. 34 the magnitude of the non-adiabatic spin torque is much smaller than that of the conventional STT (adiabatic torque).

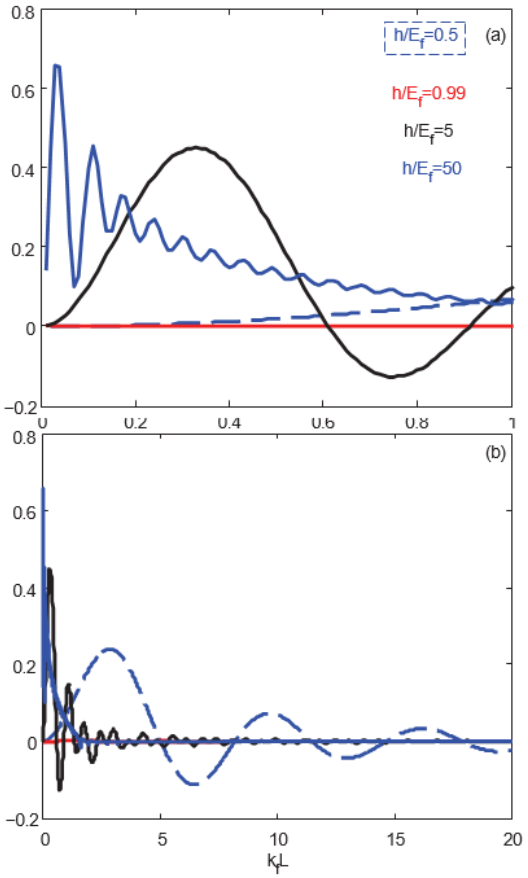

FIG.4: Color online: components of the spin transfer torque in the x-direction of spin space for different several values of k_FL versus magnetic barrier.

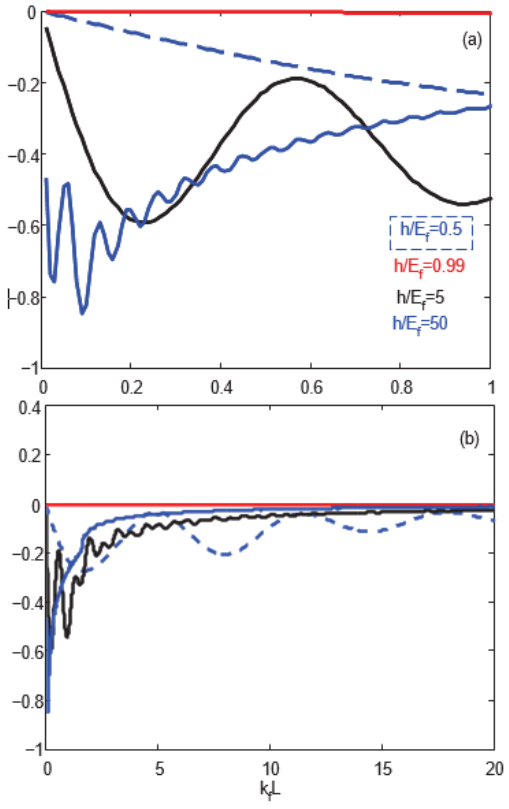

FIG.5: Color online: components of the spin transfer torque in y-direction of spin space for different values of k_FL vs.

magnetic barrier.

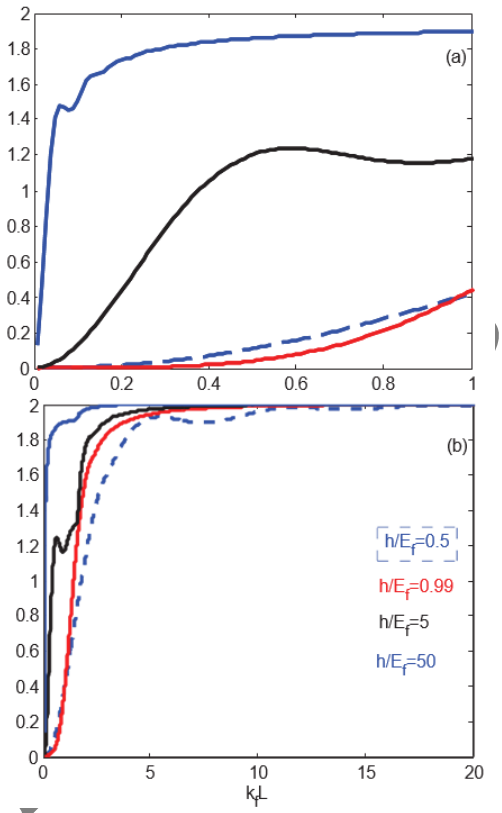

FIG.6: Color online: components of the spin transfer torque in

The components of the torque tensor has drawn for different values of magnetic barrier (ratio of exchange field to Fermi energy) versus k_FL in Figs. 4, 5, 6 from Eqs. (11,12,13). One infers from theses results that Figures divided to three regions according to ratio of exchange field to Fermi energy $\frac{h}{E_F}$.

The first noticeable point in these Figures is the oscillations in the spin transfer torque that is characteristic of graphene and also linder has pointed out it27. The results show that as k_FL increases spin torque is damping with an oscillating behavior and as the $\frac{h}{E_F}$ increases the rate of damping increases and the amount of peak of torque increases.

In reality for $h > E_F$ that junction behave like a $p-n$ junction, both adiabatic and non adiabatic torque have a high value for $k_FL < 1$ while their value for $k_FL > 1$ have a vanishing value. Due to the phenomenon of Klein tunneling, larger oscillations in spin torque than the case of $h < E_F$ is observed. The region of $h > E_F$ is important for us. This is why the speed of racetrack memory17 depend on the velocity of domain wall and correspondingly the velocity of domain wall is proportional to peak of total amount of spin transfer torque according to relation $v = \frac{g\mu_b}{nM_s} N$ where N is the peak of spin torque M_s is the saturation magnetization. More importantly in thisinterval the direction of x-torque change with increasingthe length of the DW.

Another remarkable point goes back to the Dirac point that spin transfer torque in the x and y direction of spin

space put zero36,37. This point is important that is why minimal conductance occursat the Dirac point.

For non-graphene systems non-adiabatic effects arise for short domain wall their magnitude decreases expo nentially as the wall width increases35. We have shown a method for changing the direction of DW motion. According to x-component torque seen that we can move DW parallel or antiparallel to the direction of current by adjusting the magnetic barrier and length of the DW . For istance in the interval $k_F\ L\ <1$ with $\frac{h}{E_F}=5$ and $k_F\ L$ >1 with $\frac{\mathrm{h}}{\mathrm{E_F}}=0.5$ we have change of the sign of the STT in the x-direction. We have the similar behaviour in the paper10 .

Graphene is suggested as a potentially fascinating material system rather than ferromagnetic semiconductor23 and transition metal semiconductor for manipulating magnetic patterns like DW due to having great properties like having a manipulatable magnitude of moment38 in accordance with the desired spin current density for its moving.

the z-direction of spin space for different values of k_FL versus magnetic barrier.

4. Acknowledgement

I'd like to thank Professor Saeed Abedinpour, my research supervisor, for his patient instruction, passionate support, and constructive criticisms of this study effort. Undoubtedly, doing this work without his help would not be possible

References

1. Zilber, T., Cohen, S., Fuks, D. and Gelbstein, Y., 2019. TiNiSn half-Heusler crystals grown from metallic flux for thermoelectric applications. Journal of Alloys and Compounds, 781, pp.1132-1138.
2. Kocak, B. and Ciftci, Y.O., 2018. The effect of pressure on structural, electronic, elastic, vibration and optical properties of ScXSb (X= Ni, Pd, Pt) compounds. Computational Condensed Matter, 14, pp.176-185.
3. Babalola, M.I. and Iyorzor, B.E., 2019. A search for half metallicity in half Heusler alloys. Journal of Magnetism and Magnetic Materials, 491, p.165560.
4. Inomata, K., Okamura, S., Goto, R. and Tezuka, N., 2003. Large tunneling magnetoresistance at room temperature using a Heusler alloy with the B2 structure. Japanese journal of applied physics, 42(4B), p.L419.
5. Babalola, M.I. and Iyorzor, B.E., 2021. Electronic, mechanical, vibrational and optical properties of TaIrX (X= Ge and Sn): a DFT approach. Molecular Physics, p.e1995062.
6. Goll, G., Marz, M., Hamann, A., Tomanic, T., Grube, K., Yoshino, T. and Takabatake, T., 2008. Thermodynamic and transport properties of the non-centrosymmetric superconductor LaBiPt. Physica B: Condensed Matter, 403(5-9), pp.1065-1067.
7. Chadov, S., Qi, X., Kübler, J., Fecher, G.H., Felser, C. and Zhang, S.C., 2010. Tunable multifunctional topological insulators in ternary Heusler compounds. Nature materials, 9(7), pp.541-545.
8. Van Engen, P.G., Buschow, K.H.J., Jongebreur, R. and Erman, M., 1983. PtMnSb, a material with very high magneto-optical Kerr effect. Applied Physics Letters, 42(2), pp.202-204.
9. Babalola, M.I., Iyorzor, B.E. and Okocha, O.G., 2019. Origin of half-metallicity in XCrBi (X= Hf, Ti, and Zr) half-Heusler alloys. Materials Research Express, 6(12), p.126301.
10. Webster, P.J., Ziebeck, K.R.A., Town, S.L. and Peak, M.S., 1984. Magnetic order and phase transformation in Ni2MnGa. Philosophical Magazine B, 49(3), pp.295-310.
11. Canfield, P.C., Thompson, J.D., Beyermann, W.P., Lacerda, A., Hundley, M.F., Peterson, E., Fisk, Z. and Ott, H.R., 1991. Magnetism and heavy fermion-like behavior in the RBiPt series. Journal of applied physics, 70(10), pp.5800-5802.
12. Oogane, M., Sakuraba, Y., Nakata, J., Kubota, H., Ando, Y., Sakuma, A. and Miyazaki, T., 2006. Large tunnel magnetoresistance in magnetic tunnel junctions using Co2MnX (X= Al, Si) Heusler alloys. Journal of Physics D: Applied Physics, 39(5), p.834.
13. Gautier, R., Zhang, X., Hu, L., Yu, L., Lin, Y., Sunde, T.O., Chon, D., Poeppelmeier, K.R. and Zunger, A., 2015. Prediction and accelerated laboratory discovery of previously unknown 18-electron ABX compounds. Nature chemistry, 7(4), pp.308-316.
14. Khandy, S.A. and Chai, J.D., 2021. Strain engineering of electronic structure, phonon, and thermoelectric properties of p-type half-Heusler semiconductor. Journal of Alloys and Compounds, 850, p.156615.
15. Damewood, L., Busemeyer, B., Shaughnessy, M., Fong, C.Y., Yang, L.H. and Felser, C., 2015. Stabilizing and increasing the magnetic moment of half-metals: The role of Li in half-Heusler LiMn Z (Z= N, P, Si). Physical Review B, 91(6), p.064409.
16. Kaur, K., 2017. TiPdSn: A half Heusler compound with high thermoelectric performance. EPL (Europhysics Letters), 117(4), p.47002.
17. Dasmahapatra, A., Daga, L.E., Karttunen, A.J., Maschio, L. and Casassa, S., 2020. Key Role of Defects in Thermoelectric Performance of TiMSn (M= Ni, Pd, and Pt) Half-Heusler Alloys. The Journal of Physical Chemistry C, 124(28), pp.14997-15006.
18. Zheng, W., Lu, Y., Li, Y., Wang, J., Hou, Z. and Shao, X., 2020. Structural and thermoelectric properties of Zr-doped TiPdSn half-Heusler compound by first-principles calculations. Chemical Physics Letters, 741, p.137055.
19. Gautier, R., Zhang, X., Hu, L., Yu, L., Lin, Y., Sunde, T.O., Chon, D., Poeppelmeier, K.R. and Zunger, A., 2015.

Prediction and accelerated laboratory discovery of previously unknown 18-electron ABX compounds. Nature chemistry, 7(4), pp.308-316.
20. Noda, Y., Shimada, M. and Koizumi, M., 1979. Synthesis of high-pressure phases of vanadium-cobalt-antimony (VCoSb) and vanadium-iron-antimony (VFeSb) with a dinickel-indium (Ni2In)(B82) type structure. Inorganic Chemistry, 18(11), pp.3244-3246.
21. Gu, J.B., Wang, C.J., Cheng, Y., Zhang, L., Cai, L.C. and Ji, G.F., 2015. Structural, elastic, thermodynamic, electronic properties and phase transition in half-Heusler alloy NiVSb at high pressures. Computational Materials Science, 96, pp.72-80.
22. Giannozzi, P., Andreussi, O., Brumme, T., Bunau, O., Nardelli, M.B., Calandra, M., Car, R., Cavazzoni, C., Ceresoli, D., Cococcioni, M. and Colonna, N., 2017. Advanced capabilities for materials modelling with Quantum ESPRESSO. Journal of physics: Condensed matter, 29(46), p.465901.
23. Dal Corso, A. "Elastic constants of beryllium: a first-principles investigation." Journal of Physics: Condensed Matter 28, no. 7 (2016): 075401.
24. Sarker, S., Rahman, M.A. and Khatun, R., 2021. Study of structural, elastic, electronics, optical and thermodynamic properties of Hf2PbC under pressure by ab-initio method. Computational Condensed Matter, 26, p.e00512.